Science Advances
AAAS

advances.sciencemag.org/cgi/content/full/6/31/eabc2148/DC1

Supplementary Materials for

A supramolecular platform for controlling and optimizing molecular architectures of siRNA targeted delivery vehicles

Yuting Wen, Hongzhen Bai, Jingling Zhu, Xia Song, Guping Tang*, Jun Li*

*Corresponding author. Email: jun-li@nus.edu.sg (J.L.); tangguping@zju.edu.cn (G.T.)

Published 29 July 2020, *Sci. Adv.* **6**, eabc2148 (2020)
DOI: 10.1126/sciadv.abc2148

This PDF file includes:

Section S1. Supplementary Section on Materials and Methods

1) Synthesis of host polymer CD-SS-P

CD-SS-P was synthesized using the method in our previous report (*25*). Generally, CD-SS-P polymer was prepared via atom transfer radical polymerization (ATRP) of dimethylaminoethyl acrylate (DMAEMA) monomer from β-cyclodextrin (β-CD) based macroinitiator with disulfide linkages.

Synthesis of 2-(aminoethyl) disulfanylethylcarbamoyl-*β*-CD (CD-SS-NH_2). β-CD (0.50 g, 0.44 mmol) (Sigma) was dried at 110 °C under vacuum overnight, and then dissolved in 50 mL of anhydrous DMF. After all β-CD was dissolved, the DMF solution of β-CD was dropwise to a solution of 1,1-carbonyldiimidazole (CDI) (5.67 g, 35 mmol) (Sigma) in anhydrous DMF for a period of 3 hrs under nitrogen, then the mixture was allowed to stir overnight at room temperature (R.T.). Subsequently, the resulting solution was precipitated with the mixture solution of THF (250 mL) and diethyl ether (750 mL). The precipitate was collected by centrifugation and washed with THF. Then the resulting white powder was dissolved in anhydrous DMF (50 mL) and this solution was added dropwise into cystamine dihydrochloride (7.88 g, 35.00 mmol) (Sigma) and triethylenediamine (11.78 g, 105 mmol) (Sigma) which was dissolved in anhydrous DMF (50 mL) with stirring. After this addition, the reaction mixture was stirred at R.T. for 24 hrs. The final reaction mixture was precipitated in diethyl ether. The crude product was purified by dialysis. Yield: 0.55 g, 55.6%, based on a substitution of 5. Yield: 0.55 g, 55.6%, based on a substitution of 5. ^{1}H NMR (400 MHz, d6-DMSO): δ 5.00 (brs, 7H, H-1 of β-CD), 3.30 - 3.70 (m, 48H, H-3, 5, 6a, 6b, 4, 2 of β-CD), 2.56 – 3.05 (m, 16H, -CH_2- of cystamine). By comparing the integration of the signals for the methyl protons of cystamine (-SS-CH_2CH_2-, a, b-d, 2.56-3.05 ppm) to those for the 1-positioned protons (-C(1)H) of β-CD at around 5.0 ppm, the degree of substitution (DS) was estimated. The value was calculated to be 5 for the purified CD-SS-NH_2.

Synthesis of α-bromoisobutyric amidoethyl disulfanylethylcarbamoyl-β-CD (CD-SS-Br). Briefly, to a solution of β-CD-SS-NH_2 (0.40 g, 0.2 mmol), *N*-(3-Dimethylaminopropyl)-*N'*-ethylcarbodiimide hydrochloride (EDC.HCl) (0.28 g, 1.5 mmol), *N*-Hydroxysuccinimide (NHS) (0.17 g, 1.5 mmol) in anhydrous DMSO was added 2-bromo-2-methylpropionic acid (0.20 g, 1.2 mmol). After being stirred for 24 hrs at room teperature, the reaction solution was directly dialyzed against distilled water to remove the solvent DMSO and the product was obtained by freeze dried after dialysis (MWCO 1000). Yield: 0.26 g, 43.6%, based on a substitution of 4. ^{1}H NMR (400 MHz, d6-DMSO): δ 5.00 (brs, 7H, H-1 of β-CD), 3.30 - 3.70 (m, 48H, H3, 5, 6a, 6b, 4, 2 of β-CD), 2.56 - 3.05 (m, 16H, -CH_2- of cystamine), 1.86 (s, 19H, -CH_3). By comparing the integration of the signals for the methyl protons (-C(C(e)H_3)$_2$Br, 1.86 ppm) of the initiation group to those for the 1-positioned protons (-C(1)H) of β-CD at around 5.0 ppm, the DS was estimated. The value was calculated to be 4 for the purified macroinitiator CD-SS-Br.

Synthesis of βCD-SS-pDMAEMA (CD-SS-P). CD-SS-Br (260 mg, 0.10 mmol) and dimethylaminoethyl acrylate (DMAEMA) (1.57 g, 10.0 mmol) were added into a dry flask. Tris[2-(dimethylamino)ethyl]amine (Me_6-TREN) (182.5 mg, 0.8 mmol) in 3 mL of DMSO/methanol (V/V 1:2) was added with a syringe. After de-gassing, CuBr (55 mg, 0.40 mmol) was added to the mixture. The [DMAEMA]:[CD-Br]:[CuBr]:[Me_6-TREN] relative molar ratios were 25:1:1:2. The mixture was heated at 70 °C in an oil bath. After 24 hrs, final green mixture was diluted in THF (200 mL) and passed through a short Al_2O_3 column to remove copper catalyst. The resulting

solution was concentrated and precipitated with hexane. The light yellow product was collected by centrifugation and dried under vacuum. The product was further purified by dialysis against water for 7 days (MWCO 2000), follow by lyophilized. Yield: 803 mg, 39.2%. ^{1}H NMR (400 MHz, D_2O): δ 4.10 (brs, 96H, -OCH_2- of pDMAEMA), overlapped with 3.0-4.5 (m, C(2)H-C(6)H of β-CD, 2.66 (brs, 96H, -NCH_2- of pDMAEMA), 2.26 (brs, 288H, -$N(CH_3)_2$ of pDMAEMA), 1.84 (brs, 144H, -$CBrCH_3$- of pDMAEMA), 0.62 -1.20 (m, 96H, -$CBrCH_2$- of pDMAEMA). By comparing the integration of the signals for the pDMAEMA (-$N(CH_3)_2$, around 2.26 ppm) to those for the 1- positioned protons (-C(1)H) of β-CD at around 5.0 ppm, the DP was calculated. The value was determined to be 48.

2) Synthesis of host polymer CD-P

Non-degradable host polymer without disulfide bond (CD-P) as a control compound was synthesized as follows.

Synthesis of α-bromoisobutyric β-CD (CD-Br) (*41*). β-CD (5.01 g, 4.5 mmol) was vacuum dried at 110 °C overnight. After that, it was dissolved in anhydrous N,N-dimethylacetamide (DMA) (30 mL) with stirring and then was cooled down to 0 °C. Subsequently, a solution of 2-bromo-isobutyric bromide (4.25 g, 18.0 mmol) in anhydrous DMA (10 mL) was added dropwise to the β-CD solution for a period of 1 hr at 0 °C under N_2 atmosphere. Reaction was allowed to continue at R.T. for 24 hrs. The final reaction mixture was precipitated in diethyl ether (900 mL). The resulting white powder was collected by centrifugation, washed with acetone (3×30 mL) and DI water (3×30 mL). The purified product was collected by centrifugation and lyophilized. Yield 3.93 g (50.5%, based on an average substitution degree of 4). ^{1}H NMR (400 MHz, DMSO-d6,): δ 1.88 (m, 24H, -OCO-$C(CH_3)_2$Br), 3.00-6.00 (m, 66H, -OH and -CH- of β-CD).

Synthesis of CD-P. CD-P (171.6 mg, 0.10 mmol) and DMAEMA (1.01 g, 6.40 mmol) were added into a dry flask. Me_6-TREN (146 mg, 0.64 mmol) in 3 mL of isopropanol was added with a syringe. After de-gassing, CuBr (44 mg, 0.32 mmol) was added to the mixture. The [DMAEMA]:[CD-Br]:[CuBr]:[Me_6-TREN] relative molar ratios were 16:1:1:2. The mixture was heated at 40 °C in an oil bath. After 24 hrs, final green mixture was diluted in THF (200 mL) and passed through a short Al_2O_3 column to remove copper catalyst. The resulting solution was concentrated and precipitated with hexane. The product was collected by centrifugation and dried under vacuum. The product was further purified by dialysis against water for 7 days (MWCO 2000), follow by lyophilized. Yield: 923 mg, 78.3%. ^{1}H NMR (400 MHz, D_2O): δ 4.13 (brs, 96H, -OCH_2- of pDMAEMA), overlapped with 3.0-4.5 (m, C(2)H-C(6)H of β-CD, 2.72 (brs, 96H, -NCH_2- of pDMAEMA), 2.29 (brs, 288H, -$N(CH_3)_2$ of pDMAEMA), 1.84 (brs, 144H, -$CBrCH_3$- of pDMAEMA), 0.40 -1.42 (m, 96H, -$CBrCH_2$- of pDMAEMA). By comparing the integration of the signals for the pDMAEMA (-$N(CH_3)_2$, around 2.29 ppm) to those for the 1-positioned protons (-C(1)H) of β-CD at around 5.05 ppm, the DP was calculated. The value was determined to be 48.

3) Synthesis of guest polymer Ad-PEG-FA

The procedure for synthesis of Ad-PEG4k-FA_1 from commercial PEG4.6k is given below as a typical example.

Synthesis of PEG-SS-PEG. To a solution of PEG 4k (920 mg, 0.2 mmol) and 3,3'-disulfanediyldipropanoic acid (21 mg, 0.1 mmol) in 10 mL of CH_2Cl_2 was added DCC (46 mg,

0.11 mmol) and DMAP (4 mg 0.011 mmol). The mixture was stirred at room temperature for 24 hrs. The resulting solution was filtered to remove the white precipitants and then was precipitated in cold ether. The crude product was recrystallized three times from ether and dried in vacuum, and further purified by G50 column using H_2O as the dilution. Yield: 460 mg, 48.8%.

Synthesis of Ad-PEG-SS-PEG-Ad. To a solution of PEG-SS-PEG (135 mg, 0.015 mmol) and 1-Adamantaneacetic (8.7 mg, 0.045 mmol) in 2 mL of CH_2Cl_2 was added DCC (10.31mg, 0.05 mmol) and DMAP (0.6 mg, 0.005 mmol). The mixture was stirred at room temperature for 24 hrs. The resulting solution was filtered to remove the white precipitants and then was precipitated in cold ether. The crude product was recrystallized three times from ether and dried in vacuum. Yield: 126 mg, 87.7%.

Synthesis of Ad-PEG-SH. To a solution of Ad-PEG-SS-PEG-Ad (126 mg, 0.13 mmol) in 1.6 mL of H_2O was added DTT (19.98 mg, 1.3 mmol). The mixture was stirred at room temperature for 24 hrs. The resulting solution was dried and the crude was recrystallized three times from ether. Yield: 78mg, 61.9%.

Synthesis of Ad-PEG-FA. To a solution of Ad-PEG-SH (48 mg, 0.01 mmol) and folic acid (6.6 mg, 0.015 mmol) in 1 mL of anhydrous was added EDCl (2.9 mg, 0.015 mmol), HOBt (2.1 mg, 0.015 mmol), and triethylamine (1.5 mg, 0.015 mmol). The mixture was stirred at room temperature for 24 hrs under dark. The resulting solution was directly dialyzed against distilled water to remove the solvent DMSO and the product was obtained by freeze dried after dialysis (MWCO 1000). Yield: 52 mg, 98%.

4) Synthesis of guest polymer Ad-p(PEGMA)$_m$-FA$_n$

Synthesis of Ad-p(PEGMA)$_m$. In a typical ATRP procedure, Ad-Br (31.2 mg, 0.1 mmol), determined amounts of monomer poly(ethylene glycol) monomethyl ether methacylate (PEGMA) and 2,2'-bypyridine ligand (31.1 mg, 0.2 mmol) was dissolved in 3 mL of methanol. This solution was deoxygenated before adding CuBr (14.3 mg, 0.1 mmol) into the flask. The [Ad-Br]:[CuBr]:[bpy] molar ratios were 1:1:2. The mixture was reacted at 40 ºC for 24 hrs. The final ATRP reaction mixture was directly dialyzed against deionized (DI) water using dialysis membrane with molecular weight cut-off (MWCO) of 2000 for 7 days at room temperature to remove the catalyst and unreacted macromonomer. The dialyzed solution was then filtered and freeze-dried. Yield: 0.79 g, 86%.

Synthesis of Ad-p(PEGMA)$_m$-FA$_n$. To a solution of Ad-p(PEGMA) and folic acid in a mixture of DMSO/pyridine (1:1) was added DCC (1.2 eq. to folic acid) and DMAP (0.1 eq. to folic acid). The mixture was stirred at room temperature for 1 d under dark. The crude was purified by recrystalization with ether. Products was further purified by dialysis (MWCO 2000).

Polymer characterization. Proton nuclear magnetic resonance (^{1}H NMR) spectroscopy was carried out on a 400 MHz Bruker Avance DRX NMR spectrometer. Gel permeation chromatography (GPC) analysis was performed on a Shimadzu SCL-10A system equipped with a Shimadzu RID-10A refractive index detector. Tetrahydrofuran (THF) was used as eluent. Monodispersed poly(ethylene glycol) were used as standards to obtained a calibration curve. The degree of folate functionalization was determined using UV-Vis spectrophotometer (Shimadzu UV-2450). The absorbance of folate was detected at 290 nm.

Section S2. Supplementary Section on Results and Discussion

1) Synthesis and characterization of guest polymer Ad-PEG and Ad-PEG-FA

The macromolecular guest adamantyl terminated linear Ad-PEG and Ad-PEG-FA were obtained according to the reaction scheme described in Supplementary Fig. S1a. The structures of PEG-SS-PEG, Ad-PEG-SS-PEG-Ad, Ad-PEG-SH, and Ad-PEG-FA were characterized by ^{1}H NMR spectroscopy, and the representative ^{1}H NMR spectra are shown in Supplementary Fig S1b. The adamantyl-terminated Ad-PEG molecules were also analyzed by GPC (Table S1).

2) Synthesis and characterization of guest polymers Ad-p(PEGMA)$_m$ and Ad-p(PEGMA)$_m$-FA$_{(n)}$

The macromolecular guest adamantyl-terminated Ad-p(PEGMA)$_m$ and Ad-p(PEGMA)$_m$-FA$_n$ was obtained according to the reaction scheme described in Supplementary Fig S1c. 1) The comb-shaped Ad-p(PEGMA)$_m$ hydrophilic polymers were prepared via ATRP of the monomer poly(ethylene glycol) monomethyl ether methacylate (PEGMA) using bromoisobutyryl-terminated adamantane (Ad-Br) as the initiator. 2) Folic acids were conjugated to the hydroxyl end(s) of PEG chains via carbodiimide chemistry coupling reaction.

The structures of Ad-p(PEGMA)$_m$ and Ad-p(PEGMA)$_m$-FA$_n$ were characterized by ^{1}H NMR spectroscopy, and the representative spectra are shown in Supplementary Figure S1d. The number of folic acids conjugating to Ad-p(PEGMA)$_m$ were calculated by comparing the integration signals in the region of 6.5 - 9.0 ppm corresponding to protons of aromatic groups of folate to those in the region of 3.4 - 3.7 ppm assigned to ethylene protons adjacent to ester bond of PEG chains.

The polymerization conditions and molecular characterization data for the adamantyl-terminated comb-shaped Ad-p(PEGMA)$_m$ polymers are shown in Table S2. We further conjugated various numbers of folic acids (1, 3, 6, 9, and 12) to Ad-p(PEGMA)$_m$ polymers through DCC coupling reaction. The compositions of the polymers are summarized in Table S3.

The conjugation of folate to PEG chains was further confirmed by UV-vis spectroscopy (Supplementary Figure S1e and S1f). The folate associated peak at 290 nm was found in all folate modified PEGs and the pseudo polymer formed by CD-SS-P and folate conjugated adamantyl-PEG. Moreover, the absorbance of the folate peak was positively correlated to the numbers conjugated folate. The results confirmed the folic acids were successfully conjugated to PEGs.

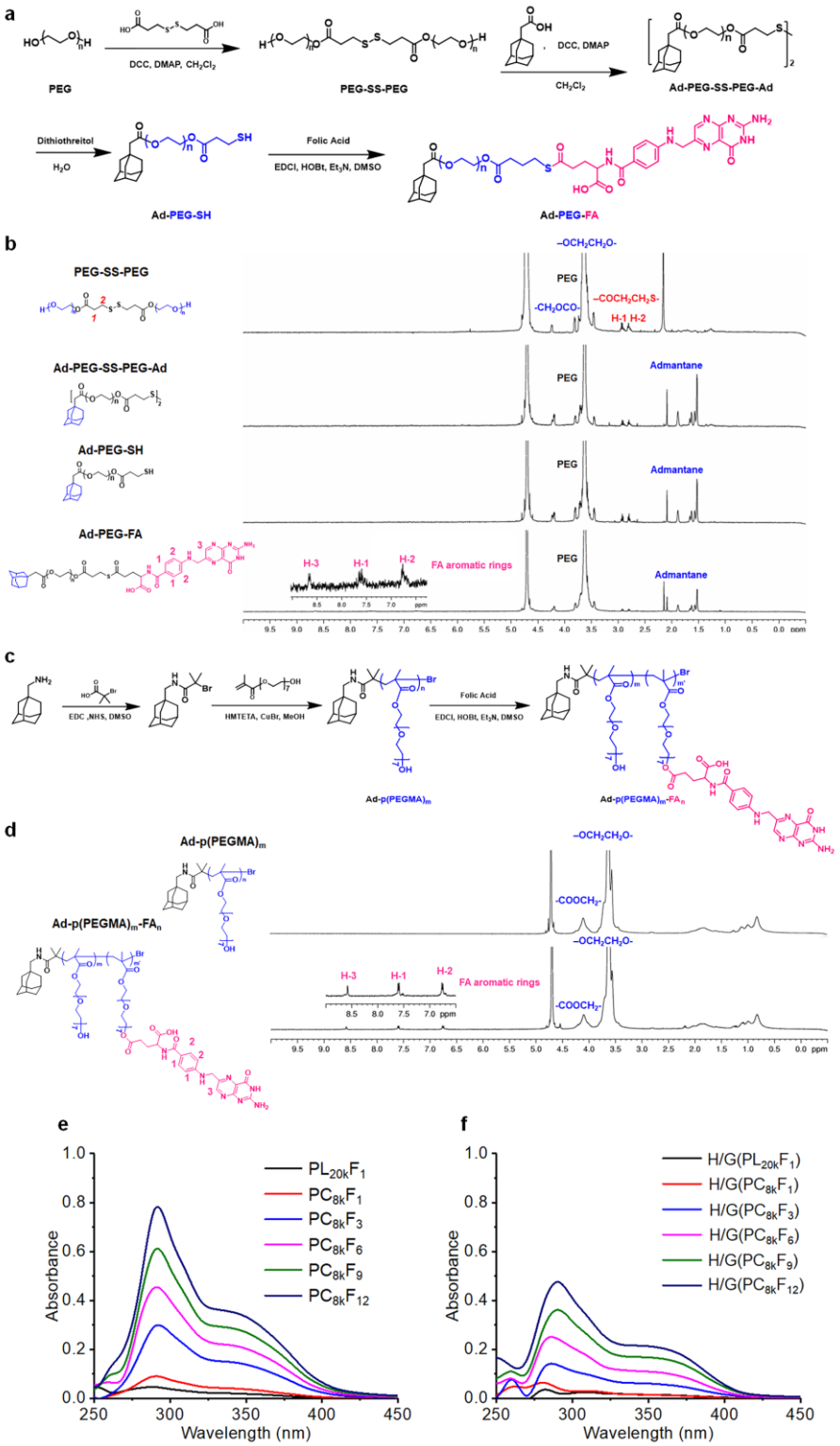

Fig. S1. Synthesis and characterization (^{1}H NMR and UV) of Ad-PEG-FA and Ad-p(PEGMA)$_m$-FA$_n$. **a**) Synthesis scheme of Ad-PEG-FA. **b**) ^{1}H NMR spectra of Ad-PEG-FA and its intermediates in D_2O (PEG molecular weight 20k). **c**) Synthesis scheme of Ad-p(PEGMA)$_m$-FA$_n$. **d**) ^{1}H NMR spectra of Ad-p(PEGMA)$_{22}$-FA$_6$ and its intermediates in D_2O. **e**) UV spectra for FA-modified guest polymers PL$_{20k}$F$_1$ and PC$_{8k}$F$_n$ (polymer concentration 2 mg/mL). **f**) UV spectra for self-assembled host-guest siRNA H/G carriers formed by CD-SS-P host polymer with PL$_{20k}$F$_1$ and PC$_{8k}$FA$_n$ guest polymers. Folate was detected at 290 nm (polymer concentration 2 mg/mL).

3) Cytotoxicity of the screened PNPs on KB cells

The cytotoxicity of all the screened PNPs were tested on KB cells. From Figure S4, the cell viability of all screened PNPs were over 90%. Comparing to PEI 25k, their cytotoxicity profile is much better, probably owing to the benefits of incorporated disulfide linkages to the siRNA delivery system. It was found that with the increase of length of PEG modifications, the cytotoxicity of PNPs slightly decreased.

4) Protein adsorption on screened siRNA encapsulated PNPs

To investigate the protein shielding effect of all the screened siRNA loaded PNPs, the protein adsorption on the particles after 24 hrs incubations were determined. It was confirmed that the PEG shielding coronas benefited to the shielding properties of the system. It must be noted that comb-like PEG and PEG with longer arms perform better in protein shielding, as compared to the linear PEG and the PEG with shorter length. Moreover, conjugation of folate to the shell of PNPs would not change its shielding ability.

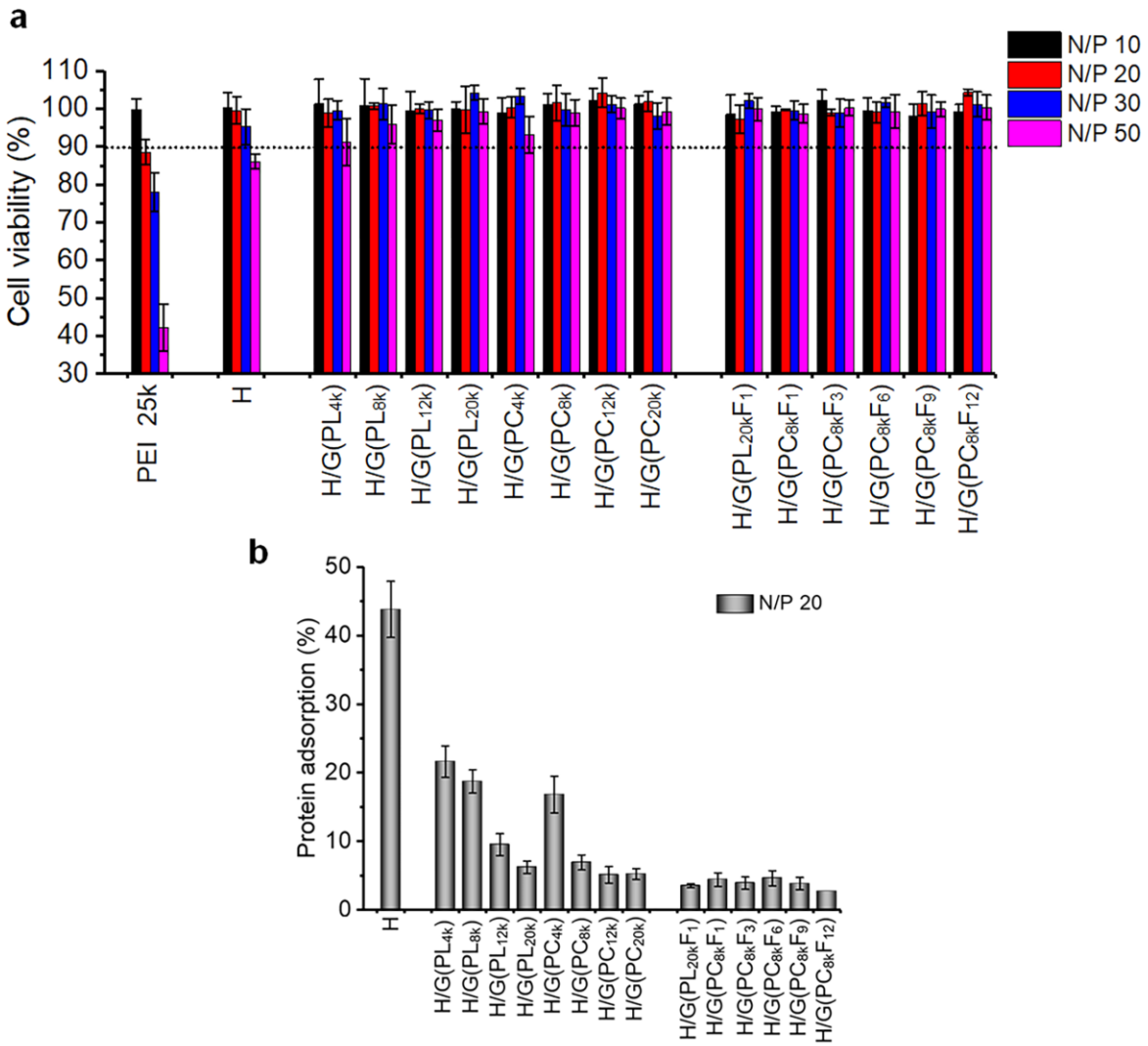

Fig. S2. Cell viability and protein adsorption. a) Cell viability of PNPs loaded with siRNA and H/G polymers at various N/P ratios were measured on KB cells. The non-shielding controls PEI 25k and H were used as the positive controls (n=4). b) Protein adsorption of PNPs with various formulations at N/P 20 (n=3).

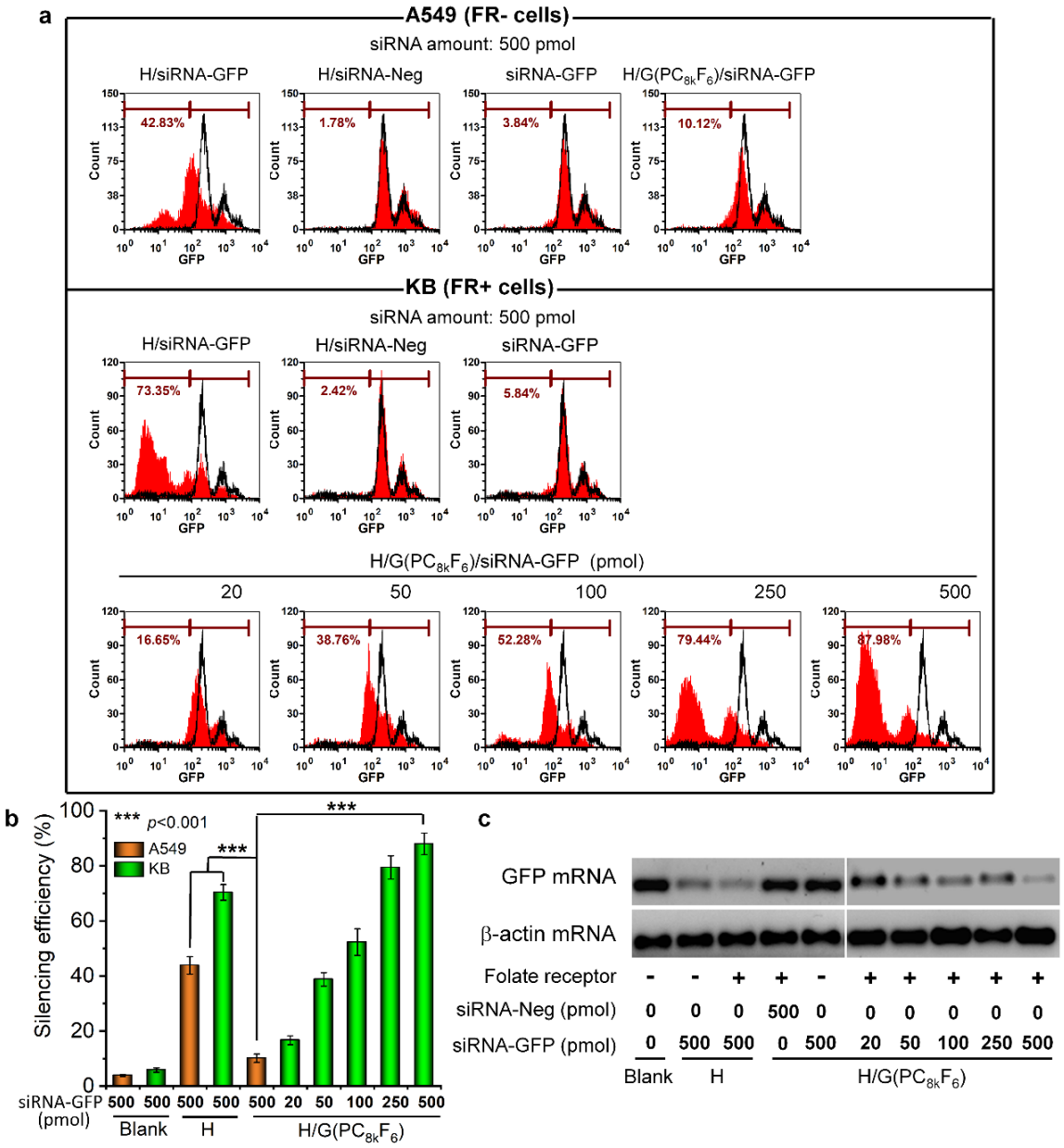

Fig S3. Silencing effect and delivery of siRNA-GFP by H or H/G($PC_{8k}F_6$) and in GFP-expressing KB-GFP and A549-GFP cells. a) Flow cytometric histograms showing the GFP expression levels. siRNA-Neg, the non-silencing siRNA, was used as the baseline of silencing effect. KB-GFP and A549-GFP cells were incubated with PNPs or naked siRNA-GFP for 4 hours, followed by additional 48 hours incubation before the GFP expression levels were measured. Black line: untreated GFP-expressing cells; Red fill: Cells transfected with indicated PNPs or naked siRNA-GFP. **b**) Silencing efficiency of H/G($PC_{8k}F_6$) in both FR+ and FR- cells. Silencing efficiency (%) = (1 – Number of cells expressing GFP after transfection / Number of cells expressing GFP before transfection) × 100%. Data were presented as mean ± S.D. (n=3). **c**) GFP mRNA levels of FR+ and FR- cells after transfection with various amounts of siRNA-GFP.

5) In vivo anti-cancer effect in KB xenograft tumour model

Images of the KB xenograft tumors of the mice at days 0 and 10 and experimental endpoint were shown in supplementary Figure S3. It was observed that tumour treated by H/G($PC_{8k}F_{6)}$ appeared smaller than other groups at all observation time points.

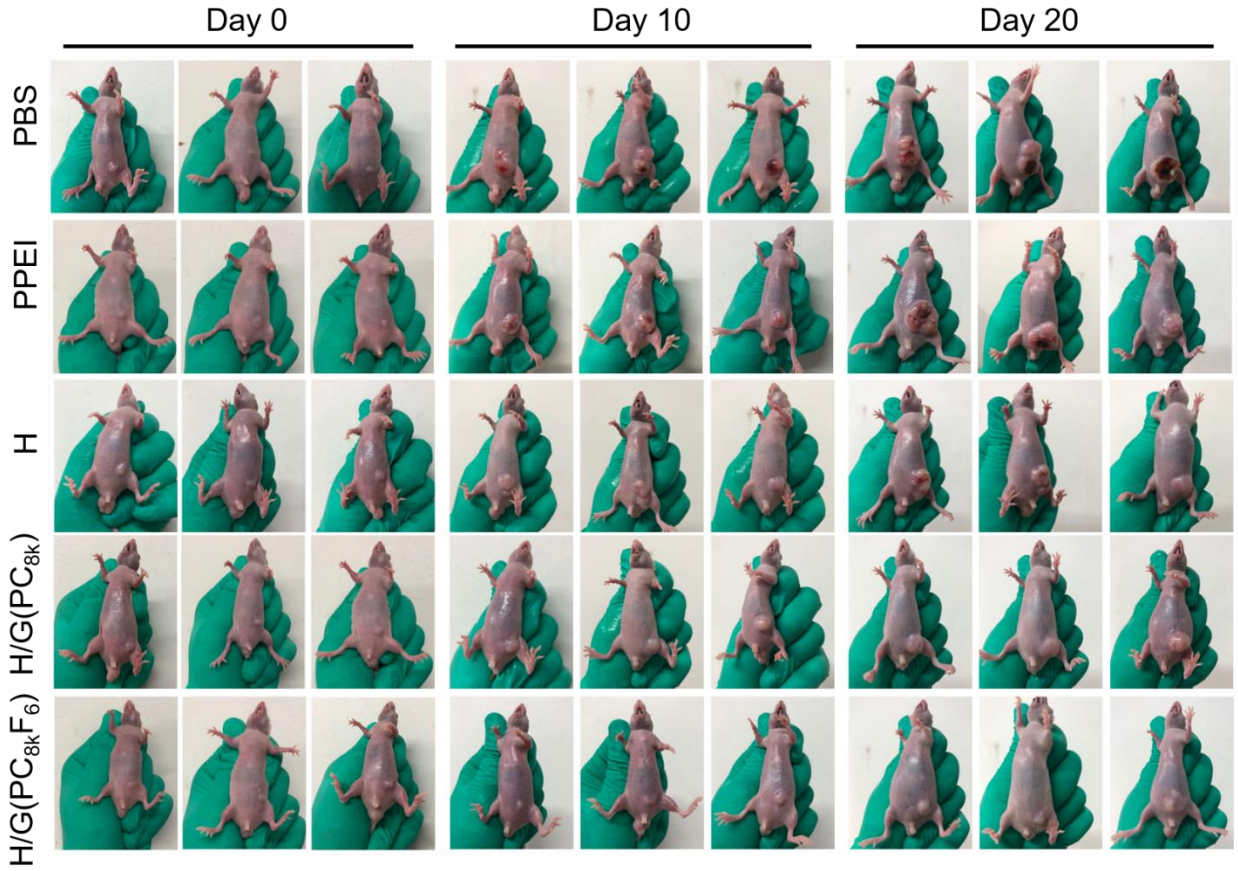

Fig. S4. Gross appearances of KB xenograft tumors of mice. Images taken at typical time points (day 0, day 10, and day 20) are shown to indicate the growth of tumor treated by different groups including PBS and other siRNA-Bcl2 loaded PNPs groups. Photo Credit: Hongzhen Bai, Zhejiang University.

6) In vivo safety profile of treatment groups

Histological sections (H&E staining, 20x) showed that no significant differences in structures of cells in liver, kidney, heart and spleen among treated and control PBS groups, suggesting that absence of acute toxicity was observed for all treatment groups.

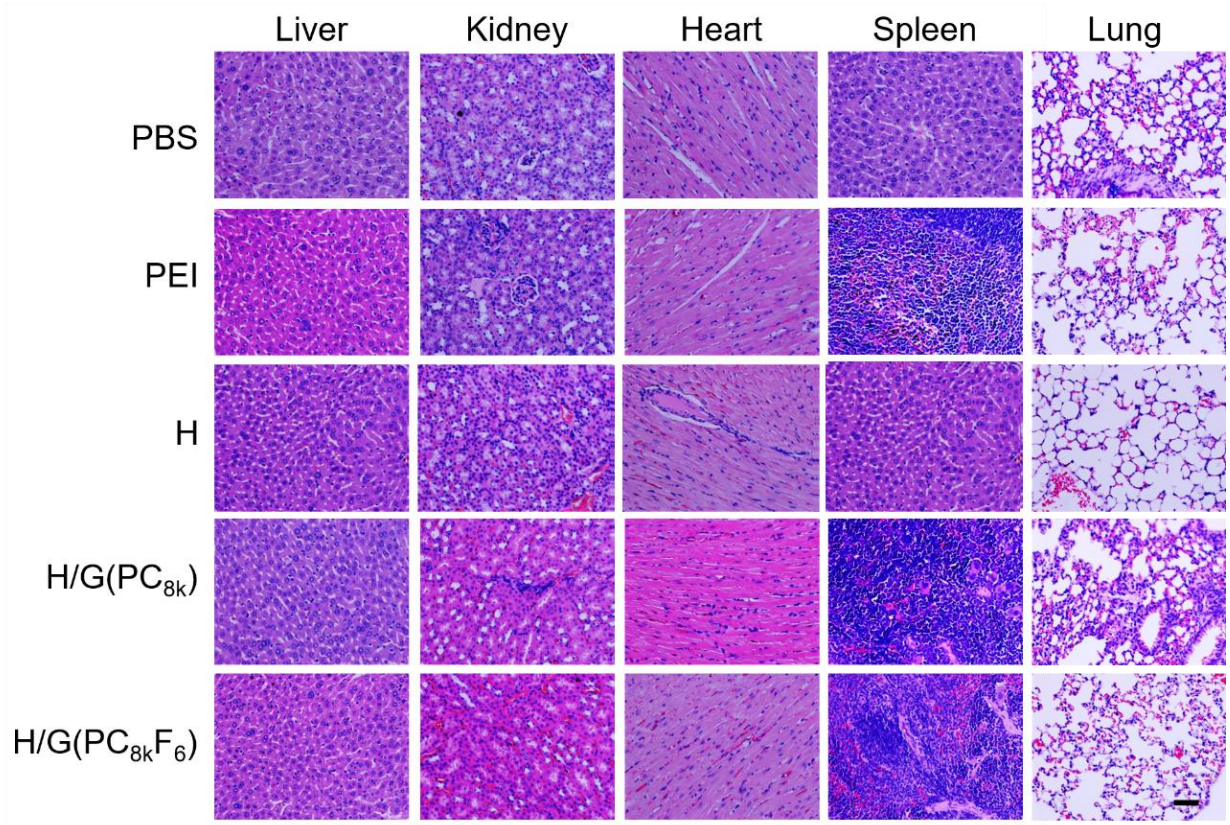

Fig. S5. Hematoxylin and erosin (H&E) staining. Representative images of H&E staining of section of formalin-fixed major organs embedded in paraffin of KB tumor bearing mice after 21-day anticancer treatment. Major organs included liver, kidney, heart, spleen and lung. Images were analyzed at 20× magnification (Scale bar = 50 μm).

To investigate whether the siRNA-Bcl2 PNPs would induce inflammatory reaction and any liver tissue injury, hematological examinations were performed for blood drawn from KB tumor bearing mice after 21-day treatment. Total protein (TP), globulin (GLO), alanine aminotransferase (ALT), aspartate aminotransferase (AST), and uric acid (UA) were examined. From Supplementary Figure S6a, all examined factors were within normal range and all treatment groups showed no significant differences from control heathy group.

To examine whether siRNA-Bcl2 loaded PNPs treatment would affect kidney functions, urine samples from KB tumor-bearing mice were examined after 21-day treatment. From Supplementary Figure S6b, no increased level of albumin and urea nitrogen in urine was observed for all groups, indicating that treatment has neglect effect on kidney functions of mice.

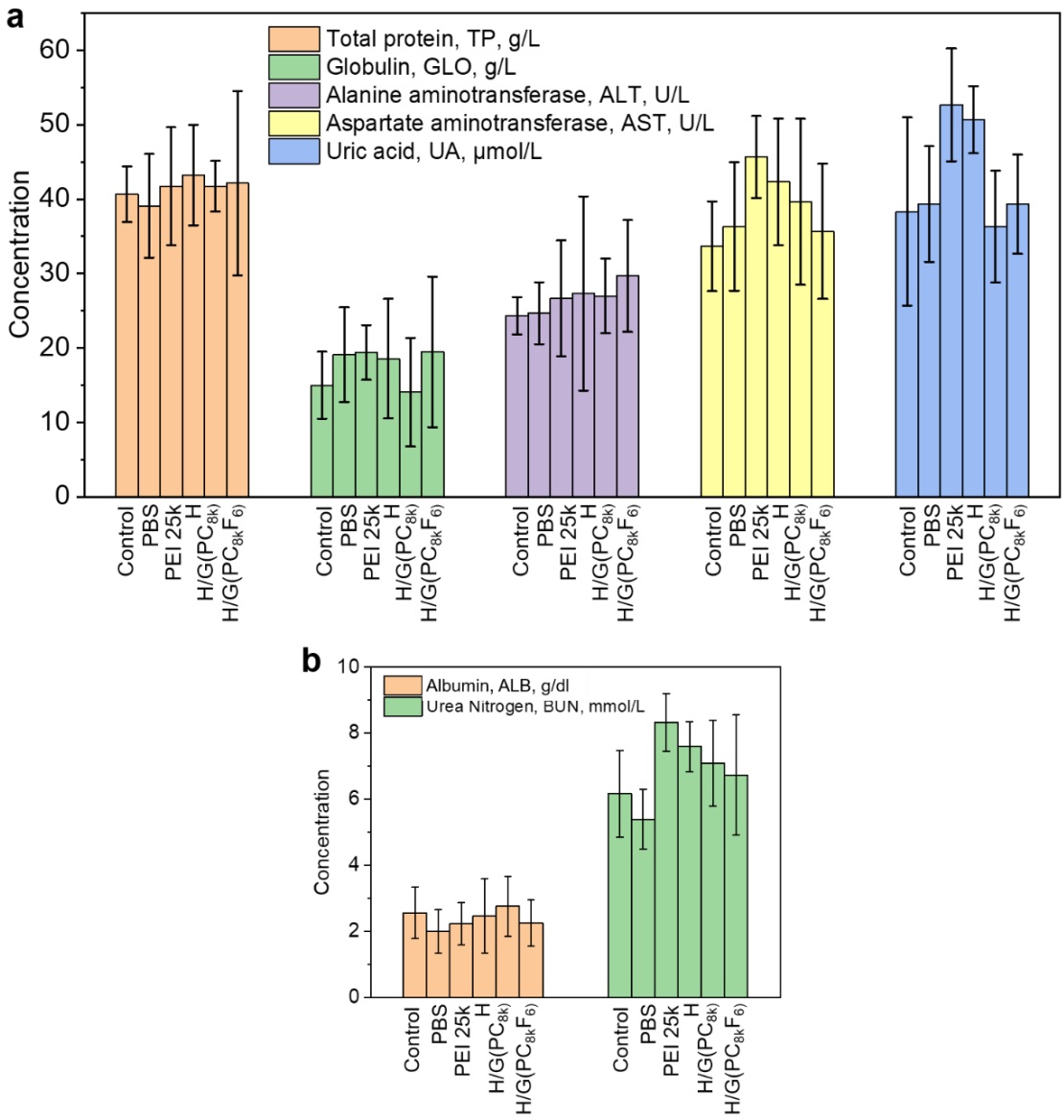

Fig. S6. Hematological and urine examinations. a) Hematological results of KB tumor bearing mice after treated with different groups including PBS and other siRNA-Bcl2 loaded PNPs groups for 21-day. After 21-day anti-tumor treatment, blood was drawn from mice and sent for hematological examination. Healthy mice without tumour were used as control. (n=3) b) Urine examination results of KB tumor bearing mice after treated with different groups including PBS and other siRNA-Bcl2 loaded PNPs groups for 21-day. Urine samples were collected from mice after 21-day anti-tumour treatment. Healthy mice without tumour were used as control. (n=3)

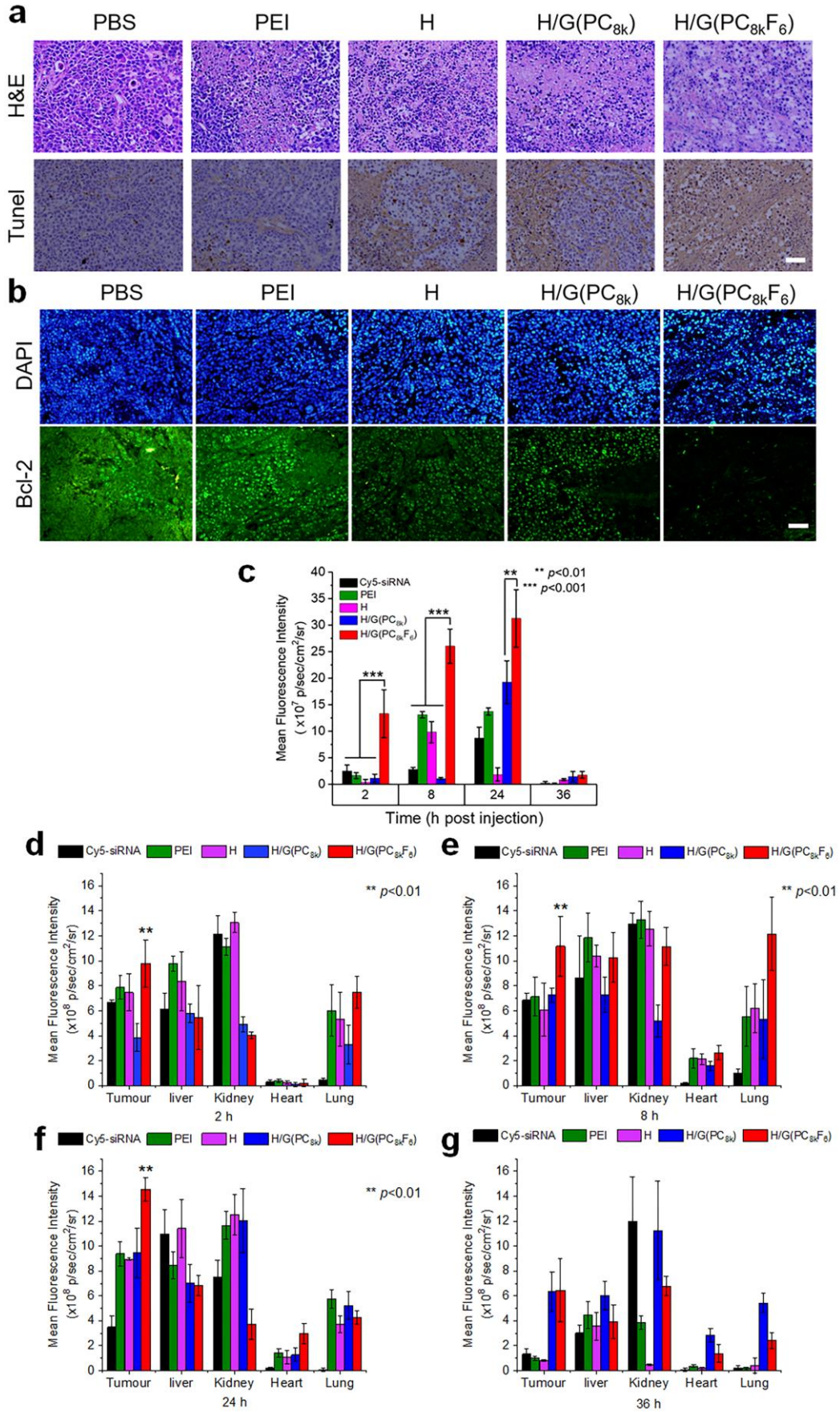
a
PBS
PEI
H
H/G(PC8k)
H/G(PC8kF6)
H&E
Tunel
b
PBS
PEI
H
H/G(PC8k)
H/G(PC8kF6)
DAPI
Bcl-2
c
Cy5-siRNA
PEI
H
H/G(PC8k)
H/G(PC8kF6)
** p<0.01
*** p<0.001
Mean Fluorescence Intensity
(x10^7 p/sec/cm^2/sr)
Time (h post injection)
2
8
24
36
d
e
f
g
** p<0.01
Mean Fluorescence Intensity
(x10^8 p/sec/cm^2/sr)
Tumour
liver
Kidney
Heart
Lung
2 h
8 h
24 h
36 h

Fig. S7. Histology and immunofluorescence staining of tumors, and fluorescence intensity of Cy5-siRNA in tumor and organs. a) Histology of KB tumors 21 days after treatment. Serial sections of formalin-fixed tumors embedded in paraffin were stained with H&E (hematoxylin and eosin) (upper row) and TUNEL (terminal deoxynucleotidyl transferase dUTP nick end labeling) (lower row), analyzed at 20× magnification (Scale bar = 50 μm). **b)** Immunofluorescence staining of Bcl-2. Cell nucleus was stained by DAPI. Green: Bcl-2 protein. Blue: nucleus. On day 21, mice were sacrificed, and their tumors resected and processed for staining. Images were analyzed at 20× magnification (Scale bar = 50 μm). **c**) Fluorescence intensity of Cy5-siRNA in tumor area at various time points. The tumor accumulation was calculated based on the quantification of Cy5 intensity in red circles. Ex vivo fluorescence imaging of tumors and main organs exploring the bio-distribution of PNPs. Fluorescence intensity of Cy5-siRNA in tumor and various major organs at **d)** 2 h, **e)** 8 h, **f)** 24 h, and **g)** 36 h post injection. Data of H/G($PC_{8k}F_6$) and H/G(PC_{8k}) groups were compared.

Table S1. Analytical results of adamantyl-terminated linear PEGs by GPC.

Name	Polymer[a]	Molecular weight, M_n	PDI[c]
		$M_{n,GPC}$[b]	
PL_{4k}	Ad-PEG_{4k}	4100	1.08
PL_{8k}	Ad-PEG_{8k}	8330	1.19
PL_{12k}	Ad-PEG_{12k}	12500	1.11
PL_{20k}	Ad-PEG_{20k}	20380	1.20

[a] Structures shown in Figure S1a.
[b] Measured by GPC, THF as the eluent.
[c] Measured by GPC, PDI = M_w/M_n.

Table S2. Polymerization conditions and molecular characterization data for adamantyl-ended comb-shaped Ad-p(PEGMA)$_m$ polymers.

Name	Polymer[a]	$[M]_0/[I]_0$	C_M [%][b]	Molecular weight, M_n			PDI[e]
				$M_{n,predicted}$[c]	$M_{n,EA}$[d]	$M_{n,GPC}$[e]	
PC_{4k}	Ad-p(PEGMA)$_{11}$	15	79.3	4200	4350.2	3900	1.20
PC_{8k}	Ad-p(PEGMA)$_{22}$	25	88.1	8300	8081.3	7400	1.22
PC_{12k}	Ad-p(PEGMA)$_{32}$	40	82.5	11800	10582.3	10300	1.16
PC_{20k}	Ad-p(PEGMA)$_{53}$	70	81.4	19600	18381.9	17800	1.15

[a] Ad-p(PEGMA)$_m$ polymers were synthesized by ATRP of poly(ethylene glycol) methacrylate (molecular weight 360).
[b] The monomer conversion was calculated based on ^{1}H NMR.
[c] The predicted M_n was calculated based on monomer conversion and $[M_0/[I]_0$.
[d] Calculated from elemental analysis-derived [N]/[C] ratio.
[e] Measured by GPC, PDI = M_w/M_n.

Table S3. Characterization of adamantyl-terminated Ad-PEG$_{20k}$-FA$_1$ ($PL_{20k}FA_1$) and Ad-p(PEGMA)$_{8k}$-FA$_n$ ($PC_{8k}F_n$).

Name	Polymer[a]	Feeding [FA]/[Ad][b]	Actual [FA]/[Ad][c]	Molecular weight, M_n / $M_{n,GPC}$	PDI
$PL_{20k}F_1$	Ad-PEG$_{20k}$-FA$_1$	1.2	1	18480	1.14
$PC_{8k}F_1$	Ad-p(PEGMA)$_{22}$-FA$_1$	1.2	1	7510	1.26
$PC_{8k}F_3$	Ad-p(PEGMA)$_{22}$-FA$_3$	4	3	7730	1.28
$PC_{8k}F_6$	Ad-p(PEGMA)$_{22}$-FA$_6$	8	6	8820	1.27
$PC_{8k}F_9$	Ad-p(PEGMA$_{22}$-FA$_9$	10	9	10850	1.21
$PC_{8k}F_{12}$	Ad-p(PEGMA)$_{22}$-FA$_{12}$	15	12	12600	1.24

[a] Folic acid was conjugated to Ad-PEG and Ad-p(PEGMA)$_{22}$ using DCC as coupling reagent in anhydrous pyridine/DMSO (v/v 1:1).

[b] The feeding ratio of folic acid to Ad-PEG or Ad-p(PEGMA) $_{22}$.

[c] The actual ratio of folate to Ad-PEG or Ad-p(PEGMA) $_{22}$ was calculated based on the ^{1}H NMR data (measured in D_2O) by comparing the integration of the signals at the region of 6.5 - 9.0 ppm corresponding to protons of aromatic groups of folic acid to those at the region of 3.45 – 3.65 ppm assigned to ethylene protons adjacent to ester bond of PEG chain.

REFERENCES AND NOTES

1. D. H. Kim, J. J. Rossi, Strategies for silencing human disease using RNA interference. *Nat. Rev. Genet.* **8**, 173–184 (2007).
2. H. J. Kim, A. Kim, K. Miyata, K. Kataoka, Recent progress in development of siRNA delivery vehicles for cancer therapy. *Adv. Drug Deliv. Rev.* **104**, 61–77 (2016).
3. M. Stevenson, Therapeutic potential of RNA interference. *N. Engl. J. Med.* **351**, 1772–1777 (2004).
4. E. Blanco, H. Shen, M. Ferrari, Principles of nanoparticle design for overcoming biological barriers to drug delivery. *Nat. Biotechnol.* **33**, 941–951 (2015).
5. H. M. Aliabadi, B. Landry, C. Sun, T. Tang, H. Uludağ, Supramolecular assemblies in functional siRNA delivery: Where do we stand? *Biomaterials* **33**, 2546–2569 (2012).
6. D. Ulkoski, A. Bak, J. T. Wilson, V. R. Krishnamurthy, Recent advances in polymeric materials for the delivery of RNA therapeutics. *Expert Opin. Drug Deliv.* **16**, 1149–1167 (2019).
7. K. A. Whitehead, R. Langer, D. G. Anderson, Knocking down barriers: Advances in siRNA delivery. *Nat. Rev. Drug Discov.* **8**, 129–138 (2009).
8. K. Tatiparti, S. Sau, S. K. Kashaw, A. K. Iyer, siRNA delivery strategies: A comprehensive review of recent developments. *Nanomaterials (Basel)* **7**, 77 (2017).
9. T. Yeung, G. E. Gilbert, J. Shi, J. Silvius, A. Kapus, S. Grinstein, Membrane phosphatidylserine regulates surface charge and protein localization. *Science* **319**, 210–213 (2008).
10. M. Miteva, K. C. Kirkbride, K. V. Kilchrist, T. A. Werfel, H. Li, C. E. Nelson, M. K. Gupta, T. D. Giorgio, C. L. Duvall, Tuning PEGylation of mixed micelles to overcome intracellular and systemic siRNA delivery barriers. *Biomaterials* **38**, 97–107 (2015).
11. Y. Fang, J. Xue, S. Gao, A. Lu, D. Yang, H. Jiang, Y. He, K. Shi, Cleavable PEGylation: A strategy for overcoming the "PEG dilemma" in efficient drug delivery. *Drug Deliv.* **24**, 22–32 (2017).
12. I. Ozer, A. Tomak, H. M. Zareie, Y. Baran, V. Bulmus, Effect of molecular architecture on cell interactions and stealth properties of PEG. *Biomacromolecules* **18**, 2699–2710 (2017).
13. C. E. Ashley, E. C. Carnes, G. K. Philips, D. Padilla, P. N. Durfee, P. A. Brown, T. N. Hanna, J. Liu, B. Phillips, M. B. Carter, N. J. Carroll, X. Jiang, D. R. Dunphy, C. L. Willman, D. N. Petsev, D. G. Evans, A. N. Parikh, B. Chackerian, W. Wharton, D. S. Peabody, C. J. Brinker, The targeted delivery of multicomponent cargos to cancer cells by nanoporous particle-supported lipid bilayers. *Nat. Mater.* **10**, 389–397 (2011).
14. E. Song, P. Zhu, S.-K. Lee, D. Chowdhury, S. Kussman, D. M. Dykxhoorn, Y. Feng, D. Palliser, D. B. Weiner, P. Shankar, W. A. Marasco, J. Lieberman, Antibody mediated in vivo delivery of small interfering RNAs via cell-surface receptors. *Nat. Biotechnol.* **23**, 709–717 (2005).

15. F. M. Mickler, Y. Vachutinsky, M. Oba, K. Miyata, N. Nishiyama, K. Kataoka, C. Bräuchle, N. Ruthardt, Effect of integrin targeting and PEG shielding on polyplex micelle internalization studied by live-cell imaging. *J. Control. Release* **156**, 364–373 (2011).
16. Y. Sasayama, M. Hasegawa, E. Taguchi, K. Kubota, T. Kuboyama, T. Naoi, H. Yabuuchi, N. Shimai, M. Asano, A. Tokunaga, T. Ishii, J. Enokizono, In vivo activation of PEGylated long circulating lipid nanoparticle to achieve efficient siRNA delivery and target gene knock down in solid tumors. *J. Control. Release* **311-312**, 245–256 (2019).
17. M. Lueckheide, J. R. Vieregg, A. J. Bologna, L. Leon, M. V. Tirrell, Structure–property relationships of oligonucleotide polyelectrolyte complex micelles. *Nano Lett.* **18**, 7111–7117 (2018).
18. C. Angell, S. Xie, L. Zhang, Y. Chen, DNA nanotechnology for precise control over drug delivery and gene therapy. *Small* **12**, 1117–1132 (2016).
19. D. R. Elias, A. Poloukhtine, V. Popik, A. Tsourkas, Effect of ligand density, receptor density, and nanoparticle size on cell targeting. *Nanomedicine* **9**, 194–201 (2013).
20. X. Song, R. Li, H. Deng, Y. Li, Y. Cui, H. Zhang, W. Dai, B. He, Y. Zheng, X. Wang, Q. Zhang, Receptor mediated transcytosis in biological barrier: The influence of receptor character and their ligand density on the transmembrane pathway of active-targeting nanocarriers. *Biomaterials* **180**, 78–90 (2018).
21. D. Bray, M. D. Levin, C. J. Morton-Firth, Receptor clustering as a cellular mechanism to control sensitivity. *Nature* **393**, 85–88 (1998).
22. E. J. Smart, C. Mineo, R. G. W. Anderson, Clustered folate receptors deliver 5-methyltetrahydrofolate to cytoplasm of MA104 cells. *J. Cell Biol.* **134**, 1169–1177 (1996).
23. X. Song, J.-l. Zhu, Y. Wen, F. Zhao, Z. Zhang, J. Li, Thermoresponsive supramolecular micellar drug delivery system based on star-linear pseudo-block polymer consisting of β-cyclodextrin-poly(N-isopropylacrylamide) and adamantyl-poly(ethylene glycol). *J. Colloid Interface Sci.* **490**, 372–379 (2017).
24. J.-l. Zhu, K. L. Liu, Y. Wen, X. Song, J. Li, Host–guest interaction induced supramolecular amphiphilic star architecture and uniform nanovesicle formation for anticancer drug delivery. *Nanoscale* **8**, 1332–1337 (2016).
25. Y. Wen, Z. Zhang, J. Li, Highly efficient multifunctional supramolecular gene carrier system self-assembled from redox-sensitive and zwitterionic polymer blocks. *Adv. Funct. Mater.* **24**, 3874–3884 (2014).
26. F. Zhao, H. Yin, J. Li, Supramolecular self-assembly forming a multifunctional synergistic system for targeted co-delivery of gene and drug. *Biomaterials* **35**, 1050–1062 (2014).

27. D. Harries, D. C. Rau, V. A. Parsegian, Solutes probe hydration in specific association of cyclodextrin and adamantane. *J. Am. Chem. Soc.* **127**, 2184–2190 (2005).
28. C. Chen, J. Ke, X. E. Zhou, W. Yi, J. S. Brunzelle, J. Li, E.-L. Yong, H. E. Xu, K. Melcher, Structural basis for molecular recognition of folic acid by folate receptors. *Nature* **500**, 486–489 (2013).
29. L. E. Kelemen, The role of folate receptor α in cancer development, progression and treatment: Cause, consequence or innocent bystander? *Int. J. Cancer* **119**, 243–250 (2006).
30. S. Hak, E. Helgesen, H. L. Hektoen, E. M. Huuse, P. A. Jarzyna, W. J. M. Mulder, O. Haraldseth, C. de Lange Davies, The effect of nanoparticle polyethylene glycol surface density on ligand-directed tumor targeting studied in vivo by dual modality imaging. *ACS Nano* **6**, 5648–5658 (2012).
31. Z. Poon, S. Chen, A. C. Engler, H.-i. Lee, E. Atas, G. von Maltzahn, S. N. Bhatia, P. T. Hammond, Ligand-clustered "patchy" nanoparticles for modulated cellular uptake and in vivo tumor targeting. *Angew Chem. Int. Ed. Engl.* **49**, 7266–7270 (2010).
32. C. He, Y. Hu, L. Yin, C. Tang, C. Yin, Effects of particle size and surface charge on cellular uptake and biodistribution of polymeric nanoparticles. *Biomaterials* **31**, 3657–3666 (2010).
33. S. Hong, P. R. Leroueil, I. J. Majoros, B. G. Orr, J. R. Baker Jr., M. M. Banaszak Holl, The binding avidity of a nanoparticle-based multivalent targeted drug delivery platform. *Chem. Biol.* **14**, 107–115 (2007).
34. K. G. Rothberg, Y. S. Ying, J. F. Kolhouse, B. A. Kamen, R. G. W. Anderson, The glycophospholipid-linked folate receptor internalizes folate without entering the clathrin-coated pit endocytic pathway. *J. Cell Biol.* **110**, 637–649 (1990).
35. R. L. Merzel, C. Frey, J. Chen, R. Garn, M. van Dongen, C. A. Dougherty, A. K. Kandaluru, P. S. Low, E. N. G. Marsh, M. M. Banaszak Holl, Conjugation dependent interaction of folic acid with folate binding protein. *Bioconjug. Chem.* **28**, 2350–2360 (2017).
36. M. Meyer, E. Wagner, pH-responsive shielding of non-viral gene vectors. *Expert Opin. Drug Deliv.* **3**, 563–571 (2006).
37. M. Shen, F. Gong, P. Pang, K. Zhu, X. Meng, C. Wu, J. Wang, H. Shan, X. Shuai, An MRI-visible non-viral vector for targeted Bcl-2 siRNA delivery to neuroblastoma. *Int. J. Nanomedicine* **7**, 3319–3332 (2012).
38. W. Sun, X.-Y. Liu, L.-L. Ma, Z.-L. Lu, Tumor targeting gene vector for visual tracking of Bcl-2 siRNA transfection and anti-tumor therapy. *ACS Appl. Mater. Interfaces* **12**, 10193–10201 (2020).
39. J. Zaias, M. Mineau, C. Cray, D. Yoon, N. H. Altman, Reference values for serum proteins of common laboratory rodent strains. *J. Am. Assoc. Lab. Anim. Sci.* **48**, 387–390 (2009).

40. N. Parker, M. J. Turk, E. Westrick, J. D. Lewis, P. S. Low, C. P. Leamon, Folate receptor expression in carcinomas and normal tissues determined by a quantitative radioligand binding assay. *Anal. Biochem.* **338**, 284–293 (2005).
41. Z.-X. Zhang, K. L. Liu, J. Li, A thermoresponsive hydrogel formed from a star-star supramolecular architecture. *Angew. Chem. Int. Ed. Engl.* **52**, 6180–6184 (2013).